Ultra-Large-Area Self-Assembled Monolayers of Nanoparticles

Tianlong Wen and Sara A. Majetich*

Physics Department, Carnegie Mellon University, Pittsburgh, Pennsylvania 15213, United States

ABSTRACT

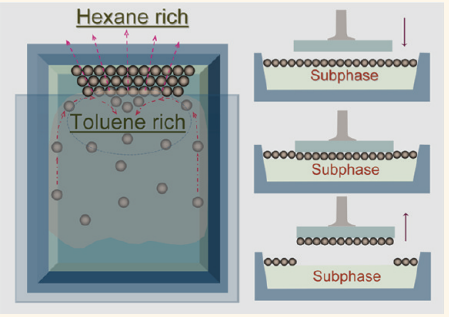

Large-area self-assembled monolayers of nanoparticles are fabricated on the surface of deionized water by controlled evaporation of nanoparticles dispersed in a binary solvent mixture. The difference in solvent volatility and partial coverage of the trough leads to a flux of nanoparticles toward the evaporation front. The monolayers are comprised of monodisperse magnetite and gold nanoparticles or slightly more polydisperse manganese oxide nanoparticles. The floating monolayers are transferred onto different substrates by the Langmuir–Schaefer method. Surfactants in the colloidal solution and substrate materials have significant impact on the monolayer formation. Bilayers of nanoparticles with different twist angles between layers are also obtained by double deposition.

KEYWORDS: self-assembly · monolayer · colloidal nanoparticles · Langmuir–Schaefer · nanopattern · bilayer Moiré pattern

Organization of large ensembles into a regular periodic pattern occurs in both natural and artificial forms.[1] Advances in nanoparticle (NP) synthesis using high boiling point organic solvent have vastly improved the control of size and shape uniformity.[2–6] The surfactant coating of these particles forms a steric barrier that prevents irreversible agglomeration of the inorganic cores. This provides the particles with the mobility needed to adjust their relative positions until they form a low-energy, self-organized pattern, such as 2D monolayers[7–10] or 3D crystals.[11–13] Among those nanopatterns, monolayers of NP assemblies are of significant technical importance in fields such as catalysis,[14] sensors,[15] nanoelectronics,[15–17] and bit-patterned magnetic media,[17–19] as well as in fundamental research.[20] However, it is a significant challenge to obtain large-area (~centimeter scale) monolayers without discontinuities.[8] When a volatile colloidal solution containing surfactant-passivated NPs is deposited on a surface, it will spread out to form a colloidal solution film. During solvent evaporation, NPs in the colloidal solution film will be driven by convective particle flux[21] to the drying front, where they dynamically adjust their relative positions to minimize their free energies. During self-assembly, NPs organize into close-packed nanopatterns with surfactant-induced gaps (~2 nm) between them to maximize their van der Waals[22] and Coulombic[23] cohesive energies. Such nanopatterns are analogous to the halftone dots arrays widely used in modern image processing.[24] As evaporation proceeds, the drying front moves toward the colloidal solution film, leaving behind assembled NP films. Such self-organization of NPs driven by solvent evaporation[25] can occur on either a solid surface[26] or a liquid surface[7] (also called a subphase). We believe ordering of NPs on a liquid surface is promising for the generation of a large area of assembled NP monolayers since this gives more freedom to NPs in the partially assembled films to adjust their positions. After solvent evaporation, the Langmuir films of self-assembled NPs will float on the surface of the subphase, which can then be transferred onto a clean substrate by the Langmuir–Blodgett[27] or Langmuir–Schaefer[28] deposition method. However, the 2D NP arrays deposited on a substrate by this method are often islands (~tens of μm) with significant gaps between them.[8] To eliminate the gaps between those islands, an isothermal compression process is often used in a Langmuir trough to push these floating islands closer on the subphase by a pair of moving barriers.[9,29] However, NP monolayers can be easily broken by mechanical force to form fractal stacks[7,26] or folded into bilayers. In previous

* Address correspondence to sara@cmu.edu.

Received for review August 8, 2011 and accepted October 19, 2011.

Published online October 19, 2011
10.1021/nn2037048

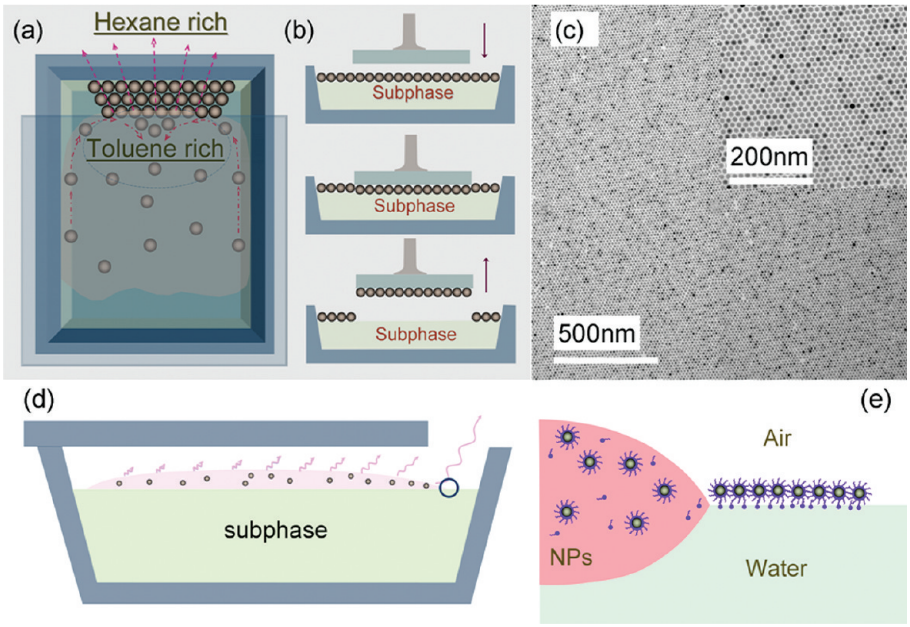

Figure 1. (a) Apparatus used to make NP monolayers on top of the subphase. The partial covering of the trough makes the organic solvent evaporate in a controllable way from the opening, and the NPs are pushed along the sidewall of the trough toward the opening from the colloidal solution reservoir from the covered region by the net solvent evaporation. At the opening, most hexane escapes to the environment, while most toluene circulates back to the colloidal reservoir. (b) After the solvent completely evaporates, a NP monolayer forms, and it is then transferred onto a substrate by the Langmuir–Shaefer method. (c) Image of such a NP monolayer deposited on a TEM grid, with the inset showing the magnified bottom left corner of the TEM image. (d) Cross-sectional schematic of the apparatus in a. (e) Autophobing process, occurring at the circled area in d, shown magnified. The functional group of surfactant in e is represented by a dot at the head of the carbon chain.

experiments, the volatile solvent in the colloidal solution film can evaporate in all directions, and the fluid flux of NPs in the colloidal solution film is uncontrolled. Here we demonstrate an easy and efficient way to generate a centimeter-sized NP monolayer without discontinuities by controlling the evaporation direction of the carrier solvent and the flux of NPs in the colloidal solution films.

RESULTS AND DISCUSSION

Iron oxide NPs are synthesized by a wet-chemical method in an organic solvent,[30] washed by ethanol, precipitated by centrifugation, and then redispersed in toluene containing a small amount of extra surfactant. Such chemically synthesized iron oxide NPs are often coated with surfactants (in our case, oleic acid), which serve as flexible spacers between them to achieve long-range order. Iron oxide NPs in toluene (~5 mg/mL) are then diluted by a factor of ~50 in a solution mixture of toluene and hexane (volume ratio 1:2). Figure 1a shows the self-assembly apparatus. A 250 μL amount of colloidal solution containing iron oxide NPs in the toluene/hexane mixture spreads into a colloidal solution film at the surface of deionized water, contained in a glass trough. The trough is then covered by a glass slide. With the combination of the glass lid and the different volatilities of toluene and hexane, the evaporation flux and fluid flux in the colloidal solution film are both well-controlled. Because the escape of vapor at the covered region is hindered, when vapor reaches the sidewall of the trough, it will be forced to flow along the sidewall toward the uncovered region. As a result, the evaporation will drive droplets containing NPs along a similar path. At the uncovered region, most of the hexane and some toluene in the droplets will quickly evaporate, while most of the toluene and some hexane will be pushed back by the fluid flux to the colloidal solution film from the center at the opening. The circulation of NP-containing droplets in the colloidal solution film can be observed by the naked eye. This circulation drives NPs to the evaporation front, where they form large-area self-assembled monolayers. The slow evaporation of toluene at the evaporation front (see toluene-rich region in Figure 1a) allows NPs to adjust their positions at the drying front to "anneal" out defects in the self-assembled monolayers and form high-quality monolayer films. In this process, the gentle and controllable fluid flux and evaporation are utilized to eliminate the gaps between NP monolayers observed in many previous experiments. After completion of the solvent evaporation in approximately 1 h, the silverish (under white light) NP monolayers are transferred from the subphase to a substrate by the Langmuir–Schaefer method, as shown in Figure 1b. Here, the Langmuir–Schaefer method is used because it is convenient for transferring the high-quality floating monolayer to the designated area. The fluid flow at the surface of the substrate

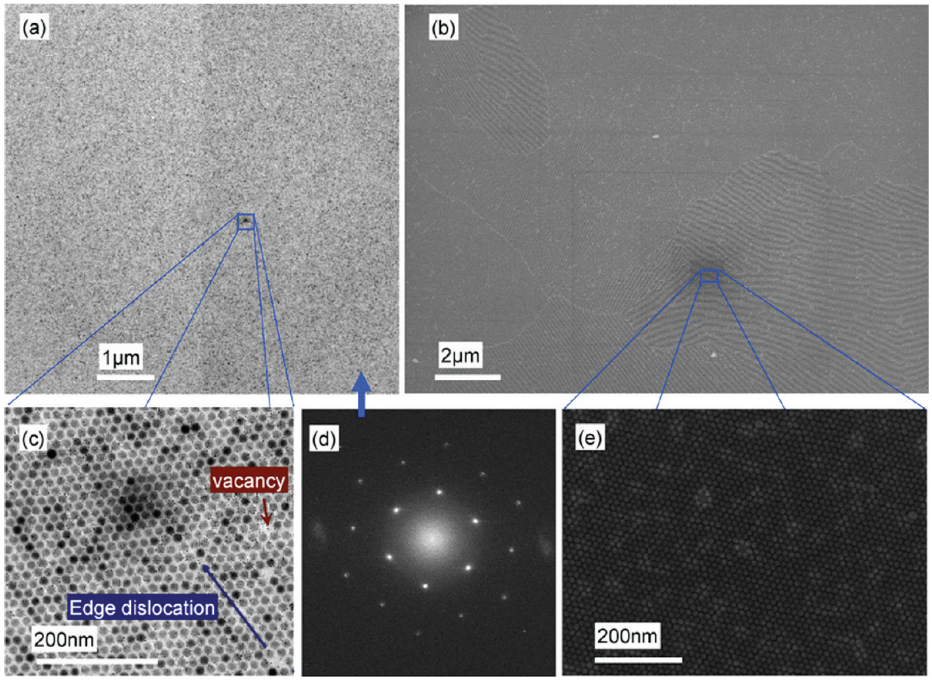

Figure 2. NPs in an area of ~7 μm × 7 μm are all aligned in a single orientation, as shown by a TEM image (a), which is confirmed by the regular hexagonal pattern of its FFT (d). As with the atomic lattices, some defects are also present, such as edge dislocations and vacancies (c). (b) A triple junction of grain boundaries of the assembled monolayers is seen by SEM. Within each grain, interference fringes are also observed for different crystal orientations. (e) A small area in b shown magnified.

during the Langmuir–Blodgett process can easily damage the fragile monolayers. While the as-made dispersion of NPs is black and opaque, the transferred NP monolayers on the substrate appear golden in color (see Figure S1 in Supporting Information). Figure 1c shows an example, made by this method, of the self-assembled monolayers of ~12 nm magnetite NPs on a carbon film mounted on a TEM grid. The largest obtained area of a continuous magnetite NP monolayer was ~3–4 cm^2.

Here a pair of low boiling point solvents, toluene and hexane, are chosen due to their different volatility and their ability to form stable dispersions of surfactant-coated NPs. When the concentration of NPs in the solution mixture is low enough, NP monolayers are often obtained, and they can be easily differentiated by the naked eye. To determine the ideal concentration of stock solution, the original solution of NPs in toluene was diluted by a factor of 100–150 in the solution mixture of toluene and hexane. NP monolayers were then made from the well-diluted solution by the above technique. The ideal concentration can be then estimated by the ratio of obtained to expected area of the NP monolayer. A high concentration of NP often results in a mixture of bilayers and multilayers of NPs, which appear different colors on water, from golden to purple under white light. A TEM image of such a multilayer is shown in Figure S2a in the Supporting Information. Monolayer formation of NPs by this method is sensitive to the mixture ratio of toluene and hexane. When the volume ratio (hexane to toluene) is ~2:1 to 1:1, NP monolayers are often obtained. Above or below this optimized ratio, bilayers or multilayers of NPs frequently occur. A toluene-rich stock solution slows the evaporation rate and leads to formation of a uniform film mixed with monolayers and bilayers (see Supporting Information Figure S2b). A hexane-rich stock solution evaporates rapidly and results in thicker multilayers. The opening at the drying front is about ~1/10 to 1/5 of the area of the glass trough. A larger opening causes evaporation to finish too quickly to obtain a well-ordered monolayer. Monolayer formation is also affected by the size, size distribution, and mass of NPs as well as concentration and aging of extra surfactant (see later discussion).

Our observations of the particle monolayer formation at the water/air interface are compatible with the deposition of material from a contact line moving below the critical velocity for film pulling. Here, the NP-containing fluid does not statically wet the water subphase because a layer of oleic acid and NP on the water surface extends beyond the contact line, forcing the spreading coefficient to be positive. This phenomenon, called autophobing, where a fluid does not wet its own monolayer, has been well-documented on solid surfaces[31,32] and speculated to occur on liquid surfaces.[33] The contact line retreat is driven by the evaporation of the solvent. By reducing the evaporation rate with our glass plate, we cause a very low contact line speed to occur. At such low speeds, no

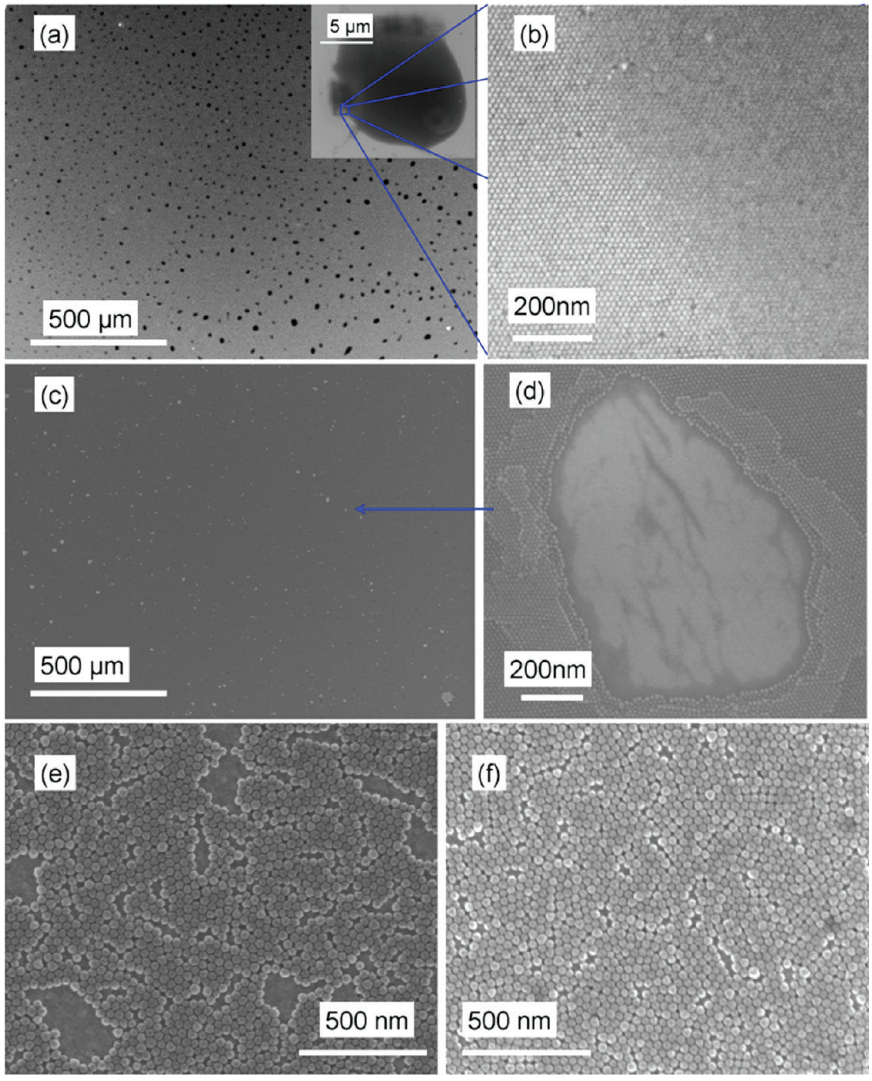

Figure 3. (a) SEM images of a ~12 nm magnetite NP monolayer deposited on a FePt thin film. Many black dots (~μm) are observed, which are surfactant aggregates. By magnifying one of the black dots (inset of a), it can be seen that the crystallinity of NP monolayers is not affected by the organic aggregate. When monolayers of the same NPs are deposited on SiO_x (c), many white spots can be observed. These white spots occur because monolayers are peeled off from the substrate by the surface tension of water during the pattern transfer (d). (e) Many empty holes are observed in the monolayer of slightly more polydisperse MnO NPs on a FePt thin film. (f) This defect density can be significantly removed by reducing the amount of surfactant in the colloidal solution.

bulk fluid film is pulled out of the meniscus as it retreats, and a monolayer of material can be continuously fed out of the contact line, as shown in Figure 1e. Such a deposition mechanism is well-known in Langmuir–Blodgett deposition for insoluble material but has also been observed for soluble materials.[34]

The monolayers produced by this method are formed at conditions close to equilibrium and have larger "grains" due to slower evaporation and nucleation in the toluene-rich regions, as depicted in Figure 1a. Here grains are defined as areas in which all NPs are aligned with a single crystallographic orientation. Figure 2a shows such a large grain with an area of ~7 μm × 7 μm, observed using a transmission electron microscope (TEM). Fast Fourier transformation (FFT) of Figure 2a is shown in Figure 2d. The pure hexagonal pattern in Figure 2d with sharp spots and multiple diffraction orders indicates that NPs in the whole ~7 μm × 7 μm area in Figure 2a are in the same grain. However, imperfections exist in any real lattice, even in atomic crystals.[35] Higher magnification of a small area in Figure 2a is shown in Figure 2c, in which several NP vacancies and an edge dislocation are present. Grain boundaries are also clearly observed in self-assembled monolayers fabricated by this technique. Figure 2b shows a triple junction of grain boundaries imaged by a scanning electron microscope (SEM). The crystallographic orientations of the monolayers are different for each grain and sometimes give rise to electron interference stripes with different periods on different grains, as clearly observed in Figure 2b. The largest period of the interference patterns in Figure 2b is

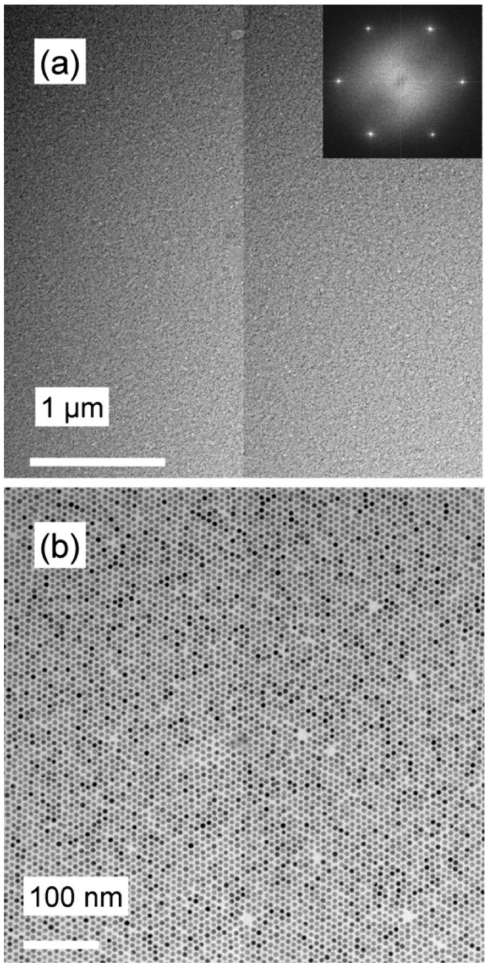

Figure 4. (a) TEM image of a monolayer of thiol-passivated Au NPs that form a single grain over an area of ~3 μm × 3 μm, as confirmed by the regular hexagonal pattern of its FFT in the inset. (b) Higher magnification of the gold NP assembly.

~200 nm. The broken interference pattern within a grain is due to the insertion of extra dislocation lines into the NP lattice. A higher magnification image of the enclosed area in Figure 2b is shown in Figure 2e. Within each grain the NP ordering is well-maintained. NP vacancies are also observed under SEM and appear brighter than the surrounding area.

The effectiveness of Langmuir film transfer from the subphase to the substrate depends strongly on the interactions between the Langmuir film and the substrate. The Langmuir film–substrate interaction is determined by the substrate material and the extra surfactant in the colloidal solutions. The latter will also affect the NP packing in the resultant monolayers. Figure 3a shows the SEM image of a large area of monolayer of ~12 nm magnetite NPs on a FePt thin film deposited on a silicon wafer. The monolayer is very uniform over the whole area of the deposited film with some isolated black dots. The inset in Figure 3a shows a magnified image of one of the black dots. The boxed region near the boundary of the black dot in Figure 3a is further magnified in Figure 3b. The crystallinity of the NP array is not disrupted across the boundary between the light and dark regions. Under SEM, darkened regions are often associated with the absorption of incoming electrons by organic materials.[36] Here the black dots in Figure 3a are attributed to extra surfactant from the colloidal solution. For Au or CdSe NPs, it is possible to adsorb a monolayer of thiol molecules and minimize the amount of excess surfactant. For metal oxide NPs, there must be some extra surfactant in the dispersion in order to maintain good equilibrium coverage of the particles and maintain colloidal stability. The black dots visible in the SEM image of the monolayers cannot be discerned under TEM (see Figure S3 in the Supporting Information) since low Z organic material is electron transparent, supporting our hypothesis. When Langmuir films transferred to SiO_x thin films by the Langmuir–Schaefer method, many white dots are observed in the SEM images, as shown in Figure 3c. One of the white dots is magnified and shown in Figure 3d. The deposited film at the white dots is peeled off from the SiO_x film and is folded back on top of the rest of the film to form a small region of bilayers, indicating reduced Langmuir film–substrate interactions. The contour of the torn monolayer matches very well that of the retained region at the broken line.

The excess surfactant aggregates could be eliminated by further washing of the colloidal solution with ethanol and the use of less surfactant. However, such "clean" monolayers are extremely difficult to transfer onto the substrate. Usually only small areas of the floating Langmuir film can be successfully transferred. Extra surfactants in the Langmuir film can increase the interaction between the Langmuir film and the substrate, thus aiding the successful transfer of the Langmuir film from the subphase onto the substrate. It was suggested that NP assembly occurs on a Langmuir layer of surfactant, which is consistent with their lower contrast in TEM images, relative to that for drop cast arrays.[9] For monodisperse iron oxide NPs, extra surfactant does not affect the crystalline structure of the arrays, but for polydisperse MnO NPs, we found the packing is affected by extra surfactant. Figure 3e and f show the assembly of polydisperse MnO NPs with and without introduction of extra surfactant, respectively, which are both deposited on FePt thin films (see large area in Figure S4 in the Supporting Information). In contrast to the monolayers of monodisperse magnetite NPs, the assemblies of polydisperse MnO NPs have glassy order. For MnO monolayers with extra surfactant (Figure 3e), many holes with missing NPs are also observed. However, after washing to remove some of the extra surfactant, the number of holes is significantly reduced, as shown in Figure 3f. The excess surfactant agglomerates and deposits on top of arrays of monodispersed iron oxide NPs, but for polydisperse MnO NPs, the agglomerates will also form in the monolayer

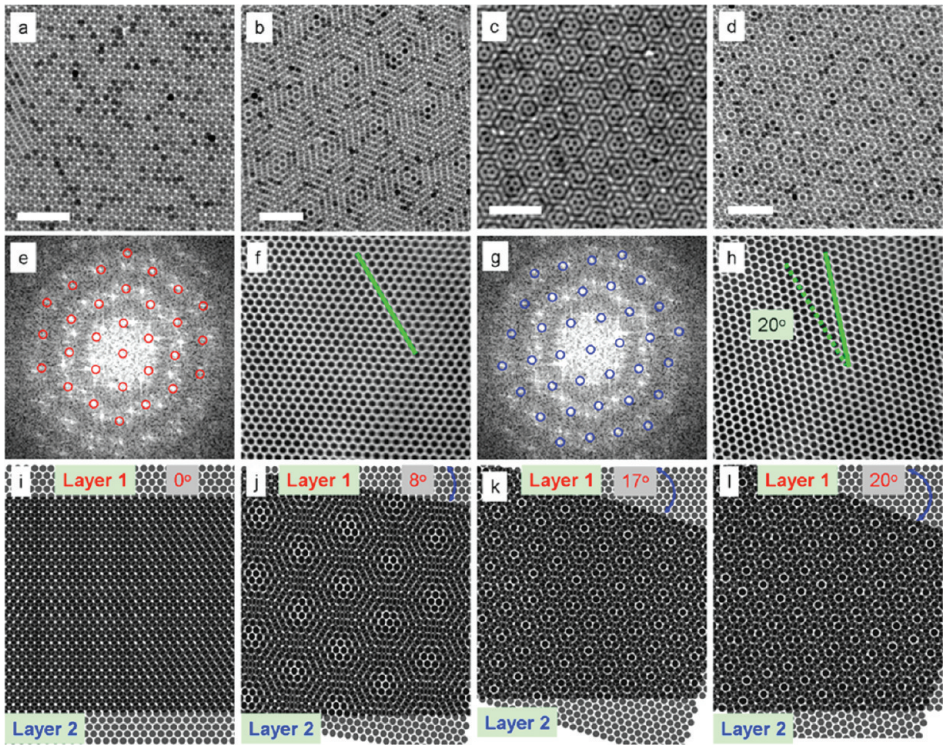

Figure 5. (a–d) Four different bilayer nanopatterns of ~12 nm magnetite NPs and (i–l) their corresponding lattice simulation, respectively. The lattice simulation is accomplished by analyzing the FFT and inverse FFT of the corresponding TEM images. For example, the FFT pattern of d can be subdivided into two sets of different patterns (e and g), which are inversely transformed back to two sets of monolayers by IFFT (f and h, respectively). On the basis of the geometry relation of the two sets of sublattices, the corresponding simulation (l) is determined. The scale bar is 100 nm.

film, disrupting the local order. The largest continuous monolayer of ~26 MnO NPs was ~10 cm^2. The observed holes in the arrays of 26 nm MnO NPs could arise from polydispersity, excess surfactant, or differences in self-assembly dynamics with larger particles. However, when polydisperse but smaller (<10 nm) particles are used, there are no holes. In addition, extra surfactant can improve the mechanical properties of the monolayers, while cracks are often observed (see Supporting Information, Figure S5) in the "clean" monolayers. The improved mechanical properties can be attributed to increased ligand–ligand interaction[37] mediated by the extra surfactant. Further, we found multilayers of NPs are often obtained even under optimized conditions due to too much surfactant, which prevents wetting of the colloidal solution on the DI water. To summarize, extra surfactants can enhance the Langmuir film–substrate interactions and thus improve the pattern transfer from the subphase to the substrate. However these extra surfactants often form aggregates in or on top of the Langmuir films.

To examine the generality of this technique for monolayer formation with surfactant-coated NPs, the process was repeated with thiol-coated gold NPs. Monodisperse gold NPs (~6 nm) were obtained by digestive ripening[38] and coated with 1-dodecanethiol as a stabilizer. Our process was found to work for Au NPs only when some extra 1-dodecanethiol was added to the toluene solution containing gold NPs. For monolayer formation, the resulting dispersion of Au NPs in toluene (1 mg/mL) was further diluted by a factor of ~10 with a mixture of toluene and hexane (volume ratio ~1:2). The same procedure used for the iron oxide NPs was applied to slowly evaporate 250 μL of the mixture in the covered trough, and then the floating film was transferred onto a substrate. This technique made large-area gold NP monolayers. The floating gold NP monolayers appear golden from above and purple when observed from the side. After transfer onto a FePt film, only a slight blue color can be discerned. Figure 4a shows a TEM image of a gold NP monolayer in an area of ~3 μm × 3 μm (see the Supporting Information, Figure S6, for an SEM image). The sharp hexagonal FFT pattern in the inset indicates that gold NPs in the whole area are all aligned along a single crystallographic orientation. The gold NP monolayer is also shown in a higher magnification in Figure 4b.

NP bilayers can be obtained by sequential transfer of two monolayers onto the substrates using the Langmuir–Schaefer method. Large-area bilayer patterns (~hundreds of nanometers) and a triple junction of bilayer domains are shown in Figure S7 in the Supporting Information. Four types of NP bilayers are shown in Figure 5a–d. To analyze the details of the bilayers, the FFT of the bilayer images is calculated. For example, the FFT of image 4d is shown in Figure 4e. It can be broken

into two subset hexagonal patterns in this FFT that are rotated by 20° relative to one another. After separately transforming back by inverse FFT (IFFT), two sets of monolayers are obtained, as shown in Figure 5f and h, respectively. The twist angle between the lattices of the two sets of monolayers is determined by the angle between the dense packing directions $\langle 2\bar{1}\bar{1}0\rangle$ (as indicated by the green line). By this method, the twist angles between the monolayers in Figure 5a–d are determined to be 0°, 8°, 17°, and 20°, respectively. To confirm that, two sets of hexagonal monolayers generated by computer are superimposed at the corresponding twist angles with respect to each others. When the twist angles are 0°, 8°, 17°, and 20°, as shown in Figure 5i, j, k, and l, the simulated bilayer patterns are very similar to those of the real image in Figure 5a, b, c, and d, respectively, which verifies the analysis. Further, upon superimposition of two NP monolayers, a Moiré pattern is obtained, as observed in the overlapping of two halftone dot arrays.[39] The period of the modulated Moiré pattern is large at low twist angle, as shown in Figure 5b and j. As the twist angle increases, the period of the modulated Moiré pattern decreases, and the cells of the Moiré pattern become smaller, as in Figure 5c and k. When the twist angle is above ~20° (Figure 5d and l), the Moiré pattern slowly becomes disordered and reaches its extreme at the maximum twist angle of 30° (see Figure S8 in the Supporting Information).

CONCLUSION

In summary, large-area self-assembled NP monolayers were prepared on an aqueous subphase by controlling the evaporation and fluid flux direction of the colloidal solution carrier fluid. This technique is performed by using two solvents with different volatility and by covering one end of the trough to control the evaporation rate and fluid flux. The floating Langmuir films were subsequently transferred onto solid surfaces by the Langmuir–Schaefer deposition method. The effectiveness of the Langmuir film deposition can be mediated by the surfactant and the substrate material. The effect of extra surfactant on the NP ordering depended on the degree of the particle monodispersity. By double deposition of NP monolayers, bilayers at different twist angles are obtained, which show different modulated Moiré patterns. The technique reported in this research work is promising for many high-tech applications, in which large-area and reliable self-assembled NP monolayers are needed. It will also make it possible to study some fundamental physics of the interparticle interactions and collective behaviors of NP monolayers or bilayers.

METHODS

Monodispersed magnetite NPs (~12 nm) were synthesized by a method first reported by Colvin and co-workers[30] that we have modified.[40] Typically, 0.178 g of iron oxyhydroxide [FeO(OH)], 2.26 g of oleic acid (OA), and 6.4 mL of 1-octadecene were stirred in a three-necked flask and degassed three times in a Schlenk line to expel oxygen. After that, the mixture was preheated at 200 °C for two hours to partially dissolve the iron precursors, followed by refluxing at 320 °C for 1 h. The mixture is cooled to room temperature, washed by ethanol, redispersed in 10 mL of toluene with addition of 50 μL of OA, and sonicated for 5 min. The washing steps were repeated five times. Magnetite NPs were finally dispersed in 10 mL of toluene with addition of 50 μL of OA. A simple estimation of the original concentration of magnetite NPs was made based on the area of the monolayer and the dilution factor. The concentration estimated by this method is ~10^{15} NPs/mL (5 mg/mL), which is roughly consistent with the more rigorous results obtained from atomic absorption spectroscopy (~6 mg/mL).

Monodisperse gold NPs (~6 nm) were synthesized by reducing Au(III) chloride hydrate [$HAuCl_4$] with sodium borohydrate [$NaBH_4$], followed by digestive ripening.[38] Specifically, 65 mg of $HAuCl_4$ and 202 mg of didodecyldimethylammonium (DDAB) were codissolved in 20 mL of toluene by sonication to form an orange solution mixture. A 0.7 g amount of $NaBH_4$ was dissolved in 2 mL of DI water. Then 100 μL of $NaBH_4$ solution was injected into the orange $HAuCl_4$ solution by pipet with vigorous stirring. Formation of gold NPs is indicated by the dark red color. After that, 1.6 mL of dodecanethiol (DDT) was added, and the mixture was stirred for 2 h to finish ligand exchange. The DDT-passivated gold NPs were then washed by 20 mL of ethanol, precipitated by centrifugation, dried under vacuum, and then redispersed in 20 mL of toluene and 1.6 mL of DDT by sonication. The solution was then refluxed in a flask with a cooling water condenser for 3 h for digestive ripening. After that, gold NPs were washed with ethanol, precipitated by centrifugation, dried under vacuum, and redispersed by sonication in 5 mL of toluene with an additional 50 μL of DDT. Finally, the solution was centrifuged for 5 min at 7000 rpm to precipitate large clusters. The top solution containing monodisperse gold NPs was then stored in a glass vial. The estimated concentration of gold NPs is ~5×10^{14} NPs/mL (1 mg/mL).

Polydispersed MnO NPs were prepared by first degassing a mixture of 15 mL of trioctylamine, 3 g of OA, and 0.692 g of manganese(II) acetylacetonate.[41] The mixture was dried under vacuum at 70 °C for 4 h, followed by quickly heating to 350 °C. During heating, a hair drier was used to prevent the acetone generated from condensing on the wall of the flask.[42] When the solution turned milky green, it was slowly cooled to room temperature and washed with the same procedure as for the iron oxide NPs. The final product was dissolved in 15 mL of toluene with addition of 50 μL of OA. The concentration of MnO NPs is ~1×10^{14} NPs/mL (7.5 mg/mL).

To prepare the stock solution for self-assembly, 120 μL of washed iron oxide NP dispersion (300 μL for MnO NPs, 600 μL for Au NPs) was added into a mixture of 2 mL of toluene and 4 mL of hexane and shaken to uniformly disperse the NPs. A glass trough was cleaned with ethanol and air-dried. A 200–250 μL portion of the colloidal stock solution was slowly injected by a syringe and spread on the surface of deionized water in the trough, which was partially covered to allow toluene and hexane to slowly evaporate into the environment, as depicted in Figure 1a. The opening is about ~1/10 to 1/5 of the area of the glass trough. After complete evaporation in ~1 h, NP monolayers float on the surface of the deionized water. Silicon wafers, coated with a thin film of either FePt or SiO_x, were sequentially washed by acetone, ethanol, and deionized water

and air-dried. The floating Langmuir films on the water were transferred onto the washed substrate or TEM grid by the Langmuir–Schaefer method, as shown in Figure 1b. The structure of NP layers deposited on silicon wafers with thin film coatings was characterized by an FEI Sirion SEM, and those monolayers deposited on TEM grids were characterized by a JEOL 2000 EX TEM.

Acknowledgment. This work has been partially supported by the U.S. National Science Foundation through Grants DMR-0804779 and CBET-0853963 and the U.S.–Israel Binational Science Foundation through Grant 2006080. The authors acknowledge Stephen Garoff (Physics, Carnegie Mellon University) for helpful discussions.

Supporting Information Available: Photographs of monolayers, TEM images of large-area self-assembled magnetite monolayer, bilayer, and multilayer obtained at unoptimized conditions, SEM images of large-area self-assembled manganese and gold monolayers, cracks in a clean monolayer, large-area bilayers, and a simulated bilayer image with a twist angle of 30°. This material is available free of charge *via* the Internet at http://pubs.acs.org.

REFERENCES AND NOTES

1. Pickover, C. A. *The Pattern Book: Fractals, Art, and Nature*; World Scientific: Singapore, 1995.
2. Peng, X. G.; Manna, L.; Yang, W. D.; Wickham, J.; Scher, E.; Kadavanich, A.; Alivisatos, A. P. Shape Control of CdSe Nanocrystals. *Nature* **2000**, *404*, 59–61.
3. Murray, C. B.; Kagan, C. R.; Bawendi, M. G. Synthesis and Characterization of Monodisperse Nanocrystals and Close-Packed Nanocrystal Assemblies. *Annu. Rev. Mater. Sci.* **2000**, *30*, 545–610.
4. Puntes, V. F.; Krishnan, K. M.; Alivisatos, A. P. Colloidal Nanocrystal Shape and Size Control: The Case of Cobalt. *Science* **2001**, *291*, 2115–2117.
5. Sun, S. H.; Zeng, H. Size-Controlled Synthesis of Magnetite Nanoparticles. *J. Am. Chem. Soc.* **2002**, *124*, 8204–8205.
6. Park, J.; An, K. J.; Hwang, Y. S.; Park, J. G.; Noh, H. J.; Kim, J. Y.; Park, J. H.; Hwang, N. M.; Hyeon, T. Ultra-Large-Scale Syntheses of Monodisperse Nanocrystals. *Nat. Mater.* **2004**, *3*, 891–895.
7. Santhanam, V.; Liu, J.; Agarwal, R.; Andres, R. P. Self-Assembly of Uniform Monolayer Arrays of Nanoparticles. *Langmuir* **2003**, *19*, 7881–7887.
8. Bigioni, T. P.; Lin, X. M.; Nguyen, T. T.; Corwin, E. I.; Witten, T. A.; Jaeger, H. M. Kinetically Driven Self Assembly of Highly Ordered Nanoparticle Monolayers. *Nat. Mater.* **2006**, *5*, 265–270.
9. Majetich, S. A.; Sachan, M.; Kan, S.; Cheng, Y.; Gardener, J. Langmuir Layers of Magnetic Nanoparticles. *Mater. Res. Soc. Symp. Proc.* **2005**, *877E*, S4.3.1–S4.3.6.
10. Collier, C. P.; Saykally, R. J.; Shiang, J. J.; Henrichs, S. E.; Heath, J. R. Reversible Tuning of Silver Quantum Dot Monolayers Through the Metal-Insulator Transition. *Science* **1997**, *277*, 1978–1981.
11. Sachan, M.; Walrath, N. D.; Majetich, S. A.; Krycka, K.; Kao, C. C. Interaction Effects within Langmuir Layers and Three-Directional Arrays of Epsilon-Co Nanoparticles. *J. Appl. Phys.* **2006**, *99*, 08C302.
12. Shevchenko, E. V.; Talapin, D. V.; Kotov, N. A.; O'Brien, S.; Murray, C. B. Structural Diversity in Binary Nanoparticle Superlattices. *Nature* **2006**, *439*, 55–59.
13. Talapin, D. V.; Shevchenko, E. V.; Kornowski, A.; Gaponik, N.; Haase, M.; Rogach, A. L.; Weller, H. A New Approach to Crystallization of CdSe Nanoparticles in Ordered Three-Dimensional Superlattices. *Adv. Mater.* **2001**, *13*, 1868–1871.
14. Lou, Y.; Maye, M. M.; Han, L.; Luo, J.; Zhong, C. J. Gold-Platinum Alloy Nanoparticle Assembly as Catalyst for Methanol Electrooxidation. *Chem. Commun.* **2001**, 473–474.
15. Shipway, A. N.; Katz, E.; Willner, I. Nanoparticle Arrays on Surfaces for Electronic, Optical, and Sensor Applications. *ChemPhysChem* **2000**, *1*, 18–52.
16. Black, C. T.; Murray, C. B.; Sandstrom, R. L.; Sun, S. Spin-Dependent Tunneling in Self-Assembled Cobalt-Nanocrystal Superlattices. *Science* **2000**, *290*, 1131–1134.
17. Majetich, S. A.; Wen, T.; Booth, R. A. Functional Magnetic Nanoparticle Assemblies: Formation, Collective Behavior, and Future Directions. *ACS Nano* **2011**, *5*, 6081–6084.
18. Hogg, C. R.; Majetich, S. A.; Bain, J. A. Investigating Pattern Transfer in the Small-Gap Regime Using Electron-Beam Stablized Nanoparticle Array Etch Masks. *IEEE Trans. Magn.* **2010**, *46*, 2307–2310.
19. Sachan, M.; Bonnoit, C.; Hogg, C.; Evarts, E.; Bain, J. A.; Majetich, S. A.; Park, J. H.; Zhu, J. G. Self-Assembled Nanoparticle Arrays as Nanomasks for Pattern Transfer. *J. Phys. D: Appl. Phys.* **2008**, *41*, 134001.
20. Puntes, V. F.; Gorostiza, P.; Aruguete, D. M.; Bastus, N. G.; Alivisatos, A. P. Collective Behaviour in Two-Dimensional Cobalt Nanoparticle Assemblies Observed by Magnetic Force Microscopy. *Nat. Mater.* **2004**, *3*, 263–268.
21. Denkov, N. D.; Velev, O. D.; Kralchevsky, P. A.; Ivanov, I. B.; Yoshimura, H.; Nagayama, K. Two-Dimensional Crystallization. *Nature* **1993**, *361*, 26.
22. Kinge, S.; Crego-Calama, M.; Reinhoudt, D. N. Self-Assembling Nanoparticles at Surfaces and Interfaces. *ChemPhysChem* **2008**, *9*, 20–42.
23. Martin, M. N.; Basham, J. I.; Chando, P.; Eah, S. K. Charged Gold Nanoparticles in Non-polar Solvents: 10-min Synthesis and 2D Self-Assembly. *Langmuir* **2010**, *26*, 7410–7417.
24. Lau, D. L.; Arce, G. R. *Modern Digital Halftoning*, 2nd ed.; CRC Press: Boca Raton, FL, 2008.
25. Rabani, E.; Reichman, D. R.; Geissler, P. L.; Brus, L. E. Drying-Mediated Self-Assembly of Nanoparticles. *Nature* **2003**, *426*, 271–274.
26. Lin, X. M.; Jaeger, H. M.; Sorensen, C. M.; Klabunde, K. J. Formation of Long-Range-Ordered Nanocrystal Superlattices on Silicon Nitride Surface. *J. Phys. Chem. B* **2001**, *105*, 3353–3357.
27. Blodgett, K. B. Films Built by Depositing Successive Monomolecular Layers on a Solid Surface. *J. Am. Chem. Soc.* **1935**, *57*, 1007–1022.
28. Langmuir, I.; Schaefer, V. J. Activities of Urease and Pepsin Monolayers. *J. Am. Chem. Soc.* **1938**, *60*, 1351–1360.
29. Tao, A. R.; Huang, J.; Yang, P. Langmuir-Blodgettry of Nanocrystals and Nanowires. *Acc. Chem. Res.* **2008**, *41*, 1662–1673.
30. Yu, W. W.; Falkner, J. C.; Yavuz, C. T.; Colvin, V. L. Synthesis of Monodisperse Iron Oxide Nanocrystals by Thermal Decomposition of Iron Carboxylate Salts. *Chem. Commun.* **2004**, 2306–2307.
31. Zisman, W. A. Relation of the Equilibrium Contact Angle to Liquid and Solid Constitution. *Adv. Chem. Ser.* **1964**, *43*, 1–51.
32. Frank, B.; Garoff, S. Temporal and Spatial Development of Surfactant Self-Assemblies Controlling Spreading of Surfactant Solutions. *Langmuir* **1995**, *11*, 4333–4340.
33. Langmuir, I. The Constitution and Fundamental Properties of Solid and Liquids. II. Liquids. *J. Am. Chem. Soc.* **1917**, *39*, 1848–1906.
34. Beppler, B. K.; Varanasi, K. S.; Garoff, S.; Evmenenko, G.; Woods, K. Influence of Fluid Flow on the Deposition of Soluble Surfactants Through Receding Contact Lines of Volatile Solvents. *Langmuir* **2008**, *24*, 6705–6711.
35. Kittel, C. *Introduction to Solid State Physics*, 3rd ed.; John Wiley & Sons, Inc.: New York, 1968.
36. Goldstein, J.; Newbury, D.; Joy, D.; Lyman, C.; Echlin, P.; Lifshin, E.; Sawyer, L.; Michael, J. *Scanning Electron Microscopy and X-Ray Microanalysis*, 3rd ed.; Kluwer Academic/Plenum Publishers: Dordrecht, The Netherlands, 2003.
37. He, J.; Kanjanaboos, P.; Frazer, L. N.; Weis, A.; Lin, X. M.; Jaeger, H. M. Fabrication and Mechanical Properties of Large-Scale Freestanding Nanoparticle Membranes. *Small* **2010**, *6*, 1449–1456.
38. Lin, X. M.; Sorensen, C. M.; Klabunde, K. J. Digestive Ripening, Nanophase Segregation and Superlattice Formation in Gold Nanocrystal Colloids. *J. Nanopart. Res.* **2000**, *2*, 157–164.
39. Lau, D. L.; Khan, A. M.; Arce, G. R. Minimizing Stochastic Moiré in Frequency-Modulated Halftones by Means of

Green-Noise Masks. *J. Opt. Soc. Am. A* **2002**, *19*, 2203–2217.
40. Lim, J.; Eggeman, A.; Lanni, F.; Tilton, R. D.; Majetich, S. A. Synthesis and Single Particle Optical Detection of Low Polydispersity Plasmonic Superparamagnetic Nanoparticles. *Adv. Mater.* **2008**, *20*, 1721–1726.
41. Ould-Ely, T.; Prieto-Centurion, D.; Kumar, A.; Guo, W.; Knowles, W. V.; Asokan, S.; Wong, M. S.; Rusakova, I.; Lüttge, A.; Whitmire, K. H. Manganese (II) Oxide Nanohexapods: Insight into Controlling the Form of Nanocrystals. *Chem. Mater.* **2006**, *18*, 1821–1829.
42. Booth, R.; Majetich, S. A. (manuscript in preparation)